

LISA Parameter Estimation Using Numerical Merger Waveforms

J.I. Thorpe¹, S.T. McWilliam¹, B.J. Kelly¹, R.P. Fahey¹, K.
A. Aamud^{1,2}, and J.G. Baker¹

¹ NASA Goddard Space Flight Center, 8800 Greenbelt Rd., Greenbelt, MD 20771,
USA

² CRESST and Department of Astronomy, University of Maryland, College Park,
MD 20742, USA

E-mail: James.I.Thorpe@nasa.gov

Abstract. Recent advances in numerical relativity provide a detailed description of the waveforms of coalescing massive black hole binaries (MBHBs), expected to be the strongest detectable LISA sources. We present a preliminary study of LISA's sensitivity to MBHB parameters using a hybrid numerical/analytic waveform for equal-mass, non-spinning holes. The Synthetic LISA software package is used to simulate the instrument response and the Fisher information matrix method is used to estimate errors in the parameters. Initial results indicate that inclusion of the merger signal can significantly improve the precision of some parameter estimates. For example, the median parameter errors for an ensemble of systems with total redshifted mass of $10^6 M_\odot$ at a redshift of $z = 1$ were found to decrease by a factor of slightly more than two for signals with merger as compared to signals truncated at the Schwarzschild ISCO.

1. Introduction

The inspiral and merger of massive black hole binaries (MBHBs) are expected to produce the strongest gravitational wave (GW) signals in the LISA frequency band. The large signal-to-noise ratios (SNRs) of these signals will allow LISA to not only detect, but measure physical parameters of the source systems. This capability will allow LISA to probe a wealth of astrophysical questions[1] including testing models of hierarchical structure formation through MBHB merger trees[2] and constraining cosmology through direct measurements of the distance-redshift relationship at high redshifts[3].

Estimates of the precision with which LISA can extract waveform parameters have been developing for the past several years, in parallel with progress in describing MBHB waveforms. Initial studies focused on equal-mass, non-spinning holes[4], while more recent analyses have added the effects of spin[5, 6] and higher harmonics[7, 8]. All of these works focus on the inspiral phase of the MBHB waveform, truncating the signals at some time before the final merger and ringdown occur.

This truncation is justified given the mechanism by which the bulk of LISA's parameter sensitivity is expected to arise, namely modulations imparted on the signal from the orbital motion of the LISA constellation [4]. Although the merger signal contributes a significant fraction of SNR, it does so in such a brief period of time that the orbital modulations have little effect on the signal, reducing its usefulness for parameter estimation. The other, more practical reason why the merger has been excluded is that the post-Newtonian (PN) approximations used to compute the waveforms break down at or near the merger and are not expected to give accurate descriptions of the merger waveform.

Numerical relativity (NR) has now provided a description of the complete waveform from inspiral through merger and ringdown [9, 10], at least for a restricted set of parameters. Analyses using hybrid PN/NR waveforms confirm that the merger portion of the signal often dominates the total SNR of a LISA MBHB observation [11]. These waveforms make it possible to check the assumption that the merger has a minimal effect on parameter estimation [12, 13]. In this paper we present an initial study of LISA parameter estimation using complete waveforms for equal-mass, non-spinning MBHBs.

2. Methodology

2.1. Waveform

The waveform used in these parameter estimation studies is a hybrid of PN and NR waveforms as described in section IV of Baker, et al. [11]. Briefly, the PN waveform (3.5PN in phase and 2.5PN in amplitude) spans the time from $2 \times 10^5 M_{\text{rest}} (G=c^3)$ to $328 M_{\text{rest}} (G=c^3)$ before the merger, where M_{rest} is the total mass of the MBHB. At $328 M_{\text{rest}} (G=c^3)$, the waveform is stitched to a NR simulation that extends through merger and ringdown. The matching time is chosen at the point where the estimated accuracy of the NR simulations exceed those of the PN expressions.

Since the hybrid waveform relies on NR simulations to generate the merger segment, it is not practical to use this technique to generate the large sets of waveforms with varying parameters that are needed for many data analysis techniques. However, if we restrict ourselves to variations in extrinsic parameters and keep intrinsic parameters such as mass ratio and hole spins fixed, it is possible to use a single "master" waveform and vary the extrinsic parameters using analytic formulae.

For our purposes, the desired waveforms are dimensionless strain in the Solar System Barycenter (SSB) frame, h_{SSB} . These depend on six extrinsic parameters: the redshifted total system mass $M = M_{\text{rest}}(1+z)$, luminosity distance D_L , coalescence time t_c , and three angles describing the orientation of the binary, in this case an inclination ι , initial orbital phase ϕ_0 , and a polarization ψ . It is convenient to construct a rescaled complex strain in the source frame, $\hat{h}_{\text{source}} = R_{\text{ext}}(h_+ + ih_-)$, which scales with M_{rest} , has a constant amplitude in the far-field limit, and can accommodate the necessary angular dependencies through rotations in the complex plane. R_{ext} is a conventional

notation for the radius at which the radiation has been extracted in the numerical simulation, although in our case, it can equally well be used as a point of reference for rescaling the PN amplitude. With these definitions, we can use the following relationship between the rescaled strain in the source frame and the dimensionless strain in the SSB, h_{SSB} :

$$h_{\text{SSB}} = \frac{r}{4} \frac{5 G M}{c^2 D_L} e^{2i} \hat{h}_{\text{source}} \cos^4 \frac{\theta}{2} e^{2i\phi} + \hat{h}_{\text{source}} \sin^4 \frac{\theta}{2} e^{2i\phi} \quad (1)$$

Two additional extrinsic parameters describe the sky location of the binary in the SSB frame. In this case we use galactic longitude and latitude. The effect of these parameters of the waveform is handled by the instrument model, described in the next section. In total, our model uses eight extrinsic parameters to determine h_{SSB} from \hat{h}_{source} . In the remainder of this work, the vector $\tilde{\mathbf{p}} = (M; D_L; \iota; \phi; \phi_0; \iota_c)$ denotes these parameters and the shorthand notation $h = h(\tilde{\mathbf{p}})$ represents the transformation in (1).

2.2. Instrument Model

There are two necessary components for modeling the sensitivity of a gravitational wave detector [14]: a response function relating the gravitational wave signal to the instrument output and a noise model describing all other components of the instrument output.

In the case of LISA, the instrument outputs are the Time Delay Interferometry [15, 16] (TDI) streams. TDI is a technique by which the differential phase measurements made at each spacecraft are combined with appropriate time delays in order to form outputs for which laser phase noise is canceled but GW signals remain. For data analysis purposes, it is convenient to use a set of "optimal" TDI channels [17] that form an orthogonal basis in the TDI signal space. For an optimal set, each channel contains independent noise and can therefore be treated as a separate detector. We have defined a set of optimal channels $A = (A^0; E^0; T^0)$ where $A^0 = \frac{1}{2} \frac{1}{\sqrt{2}} (Z - X)$, $E^0 = \frac{1}{2} \frac{1}{\sqrt{6}} (Z + X - 2Y)$, and $T^0 = \frac{1}{2} \frac{1}{\sqrt{3}} (Z + X + Y)$ where $(X; Y; Z)$ are the first-generation Michelson TDI variables. The primed notation is used to distinguish A from the $(A; E; T)$ used by Prince, et al. [17].

The Synthetic LISA software package [18] is used to model the instrument response to the GW signal. Synthetic LISA models the orbits of the individual spacecraft and computes the constellation geometry. The GW response in each arm is then computed and assembled to form the appropriate TDI combinations. Although the computational cost of a numerical simulation exceeds that of an analytic model, the Synthetic LISA model provides higher fidelity, particularly at high Fourier frequencies where the instrument response becomes complex and time-dependent.

It would also be possible to use Synthetic LISA to compute the noise output in the A channels as well as the signal response. The difficulty with this approach is that statistical variations cause the noise curve to change from one run to the next, washing out the subtle changes corresponding to variations in waveform parameters. This effect

could be mitigated by averaging repeated simulations with varying seeds, however this would add to the computational cost.

An alternative approach, the one taken by most estimates of LISA sensitivity in the literature, is to derive an analytic expression for the average noise level in a TDI channel given the noise spectra of the individual components. For A, the one-sided power-spectral densities (PSDs) of the noise are given by

$$S_{A^0 E^0} = 2 \sin^2(\alpha) [f^2 (3 + 2 \cos(\alpha) + \cos(2\alpha))] S(f) + [2 + \cos(\alpha)] S_{\text{op}}(f) g; \quad (2)$$

$$S_{T^0} = 8 \sin^2(\alpha) \sin^2(\alpha/2) 4 \sin^2(\alpha/2) S_{\text{pm}}(f) + S_{\text{op}}(f); \quad (3)$$

where $2fL=c$, f is the Fourier frequency, L is the average detector arm-length, and $S_{\text{pm}}(f)$ and $S_{\text{op}}(f)$ are the strain-equivalent proof-mass acceleration and optical-path noises of the LISA links respectively. For this work, $S_{\text{pm}}(f) = 2.5 \cdot 10^{-48} \text{ Hz}^{-1}$ ($f=1 \text{ Hz}$) $1 + (f=0.1 \text{ mHz})^4$ and $S_{\text{op}}(f) = 1.8 \cdot 10^{-37} \text{ Hz}^{-1}$ ($f=1 \text{ Hz}$).

In addition to the noise introduced by the instrument, MBHB signals are also partially obscured by a "foreground" of other GW signals. This foreground is composed of a superposition of tens of thousands of compact binaries in our galaxy and its neighborhood. We estimate the noise contribution in A^0 and E^0 of this stochastic foreground as $S_{\text{gal}}(f) = [4 \sin^2(\alpha)] S_{\text{conf}}(f)$, where $S_{\text{conf}}(f)$ is taken from equation (14) of Tinpano, Rubbo, and Comish [19]. The pre-factor in $S_{\text{gal}}(f)$ is an estimate of the signal response functions of A^0 and E^0 for the frequencies where $S_{\text{conf}}(f)$ is defined, $40 \text{ Hz} \leq f \leq 8 \text{ mHz}$. At these low frequencies, the response in the T^0 channel is near zero. Consequently no foreground is added to the T^0 channel.

One downside to using different instrument models for the signal and the noise is that artifacts can arise when these models are inconsistent. For example, the analytic formulas predict zero noise at $f_n = nc/L$; $n = 1; 2; 3; \dots$. Were analogous formulae used to predict the signal response, the result would be zero signal at $f = f_n$. In practice, the Synthetic LISA model predicts some finite signal at $f = f_n$, partly due to errors in estimating PSDs from discrete time series. The result is an infinite contribution to the SNR at $f = f_n$. To alleviate this problem, we added an artificial "floor" of 10^{-40} Hz^{-1} ($f=1 \text{ Hz}$) to the noise models for A.

The T^0 channel has a related problem at low frequencies, where $S_{T^0} \propto f^2$. The corresponding signal response function should also fall off with f^2 at low frequencies in order for SNR to converge. In practice, the T^0 channel response for our signals leveled off at a finite value, leading to an erroneous increase in SNR (and parameter sensitivity). It may be possible to address the problem with the T^0 channel by adding an artificial noise floor to $S_{T^0}(f)$ or by only using it in the high-frequency limit. For this work, however, we have chosen to neglect the contributions of the T^0 channel until the issue can be further investigated.

Finally, we note that these types of artifacts may arise when actual instrumental data is analyzed. Most analysis methods require some model of the instrument response and noise, each of which will have some discrepancies with the actual instrument

behavior.

2.3. Parameter Sensitivity Calculation

With the waveform described in Sec. 2.1 and the instrument model described in Sec. 2.2 in hand, the next step is to develop a procedure for evaluating parameter sensitivity. Like many others in the community, we have selected the Fisher information matrix approach [20].

The steps for the approach are as follows. A SSB waveform with a particular set of extrinsic parameters $\tilde{\alpha}_0$ is generated from the master waveform, $h_0 = h_{\text{SSB}}(\tilde{\alpha}_0)$. A set of perturbed waveforms is then generated by perturbing each of the parameters individually, $h_i = h_{\text{SSB}}(\tilde{\alpha}_0 + \delta_i \hat{e}_i)$, where δ_i is the size of the perturbation in the i th parameter direction. The instrument response to h_0 and h_i is computed using Synthetic LISA. The partial derivative of the instrument response with respect to each parameter is then estimated using a one-sided difference,

$$\frac{\partial A}{\partial \tilde{\alpha}_i} \bigg|_{\tilde{\alpha}=\tilde{\alpha}_0} = \frac{A_i - A_0}{\delta_i} \quad (4)$$

where A_0 is the response to h_0 and A_i is the response to h_i . These parameter derivatives are used to estimate the Fisher information matrix

$$F_{ij} = \frac{\partial A}{\partial \tilde{\alpha}_i} \frac{\partial A}{\partial \tilde{\alpha}_j} \quad (5)$$

where $(a|b)$ denotes the noise-weighted inner product,

$$(a|b) = 2 \int_0^Z \frac{a^*(f)b(f) + a(f)b^*(f)}{S_n(f)} df \quad (6)$$

The quantity $S_n(f)$ is the PSD of the appropriate TDI channel. In our case we estimate the Fourier transform of $\partial A / \partial \tilde{\alpha}_i$ from the time series using a discrete Fourier transform with tapering applied to the early and late portion of the signal to reduce spectral artifacts. The inner product in (6) is evaluated as a discrete sum with finite upper and lower integration limits.

Since the A channels are constructed to be linearly independent, it is appropriate to sum their individual Fisher matrices to yield the effective Fisher matrix for the instrument as a whole. However, as discussed in section 2.2, the T^0 channel was not well-behaved in our instrument model. For that reason, we have omitted the T^0 channel and defined the composite Fisher matrix as $F_{ij} = F_{ij}^{(A)} + F_{ij}^{(E)}$. Taking the usual limit of large SNR, we compute the covariance matrix $C_{ij} = (F^{-1})^{ij}$ and parameter errors $\sigma_i = \sqrt{C_{ii}}$. In order to explore the effect of the choice of $\tilde{\alpha}_0$, we perform multiple runs with varying $\tilde{\alpha}_0$ and estimate the probability density functions of $\tilde{\alpha}^{ij}$ and σ_i .

3. Results

For our initial trials, we choose an ensemble of 140 systems, each with $M = 10^6 M_\odot$ and $D_L = 6 \text{ Gpc}$, corresponding to $z = 1$ in standard Λ -CDM cosmology. The remaining

Table 1. Mean and median values for parameter errors and SNR for an ensemble of 140 equal-mass, non-spinning binaries with $M = 10^6 M_\odot$ at $D_L = 6 \text{ Gpc}$ ($z = 1$). For ‘pre-ISCO’, integrations of Fisher matrix elements were cut off at a frequency corresponding to Schwarzschild ISCO.

| | total mean | pre-ISCO mean | total median | pre-ISCO median |
|--------------------------|-----------------------|-----------------------|-----------------------|-----------------------|
| SNR_{AE} | 1.12×10^3 | 8.35×10^2 | 9.28×10^2 | 6.98×10^2 |
| $\ln(M/M_\odot)$ | 2.35×10^{-6} | 4.00×10^{-6} | 1.66×10^{-6} | 3.26×10^{-6} |
| $\ln(D_L/1 \text{ pc})$ | 3.78×10^{-1} | 6.07×10^{-1} | 4.48×10^{-2} | 1.18×10^{-1} |
| ι (deg) | 3.84 | 7.19 | 2.15 | 5.28 |
| δ (deg) | 17.7 | 26.9 | 4.64 | 9.19 |
| α (deg) | 81.9 | 137 | 1.08 | 3.12 |
| ϕ (deg) | 607 | 1270 | 1.59 | 4.26 |
| ψ (deg) | 620 | 1290 | 7.46 | 15.9 |
| t_c (sec) | 17.1 | 39.5 | 6.87 | 27.3 |

parameters (ι , δ , α , ϕ , ψ , and t_c) were randomly varied over the ensemble. For each member of the ensemble, χ^2_{ij} was computed using two different upper frequency limits for the inner product in (6). In one case, the integral was truncated at the Schwarzschild inner-most stable circular orbit (ISCO) frequency whereas in the second case it was continued for an order of magnitude beyond the peak (merger) frequency. Table 1 lists the mean and median values of the SNR and parameter errors for the ensemble. Histograms of each parameter error for both cases are shown in Figure 1. Note that the plotted quantities are the direct results of the technique outlined in 2, without imposing any physical limits on the sizes of the errors. For example, an error in galactic latitude of 1000 deg should be interpreted as the measurement providing no useful information for that system.

The median improvement in χ^2_i upon inclusion of the merger is a factor of ~ 2 , with the exception of t_c , which improves by a factor of ~ 4 . In all cases, the improvement factor is greater than that for the median SNR of $\sim 25\%$, suggesting that most of the improvement is via a mechanism other than direct increase in SNR.

One possible mechanism is that a pair of parameters that is nearly degenerate in the inspiral phase becomes decoupled in the more complex merger phase of the waveform. Table 2 lists the percentage decrease in covariance for each parameter pair from pre-ISCO to total waveform. Note that all of the covariances decrease when the post-ISCO waveform is added. Covariances with the coalescence time exhibit the most dramatic decrease. This can be qualitatively explained by arguing that the merger provides a sharp feature that constrains the coalescence time more tightly and breaks degeneracies with other parameters.

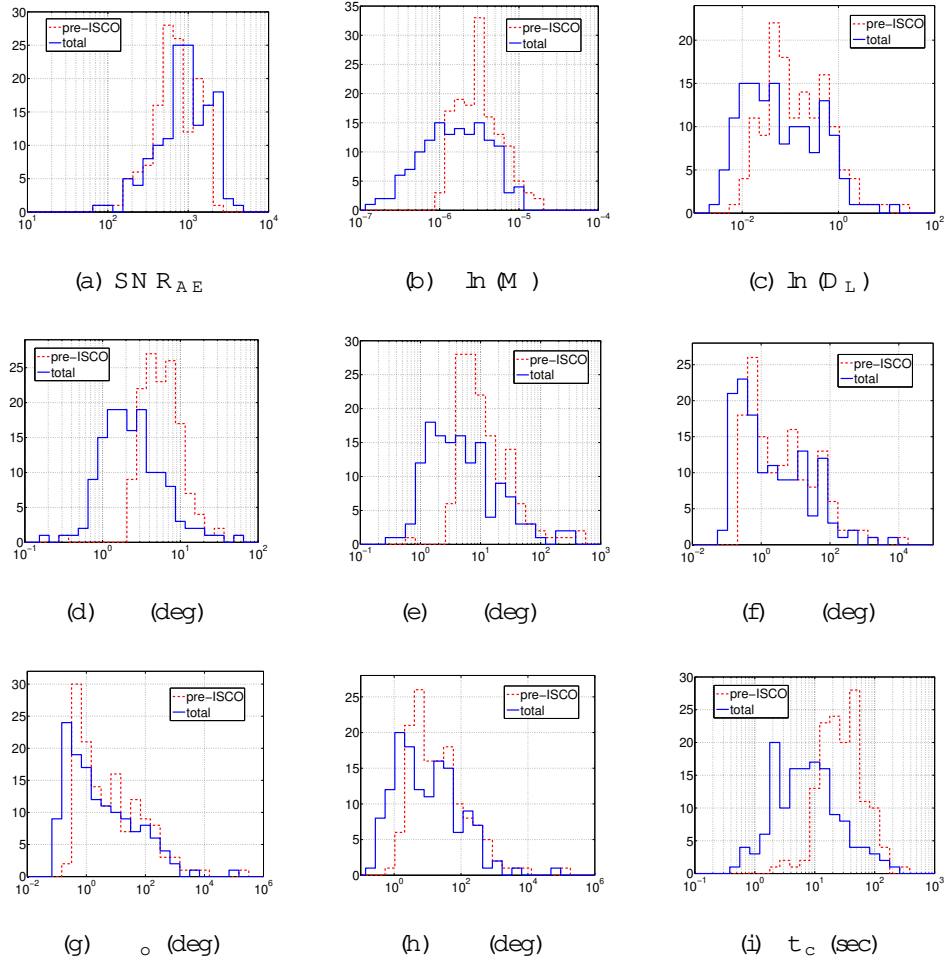


Figure 1. Histograms of SNR and i for ensemble summarized in Table 1. The dashed lines are the results with a cutoff at ISCO, the solid lines include the entire waveform.

Table 2. Median percentage reduction in covariance from pre-ISCO to total signal, $1 - \frac{\text{cov}_{ij}(\text{total})}{\text{cov}_{ij}(\text{pre-ISCO})}$.

| | $\ln M$ | $\ln D_L$ | | | | ϕ | | t_c |
|-----------|---------|-----------|------|------|------|--------|------|-------|
| $\ln M$ | 72.3 | 70.8 | 63.5 | 90.7 | 71.4 | 79.2 | 82.4 | 91.1 |
| $\ln D_L$ | — | 75.7 | 79.6 | 82.3 | 76.4 | 83.5 | 83.4 | 95.4 |
| | — | — | 80.9 | 89.6 | 80.8 | 77.2 | 81.9 | 97.6 |
| | — | — | — | 82.9 | 83.1 | 80.8 | 81.8 | 87.2 |
| | — | — | — | — | 76.8 | 87.0 | 86.6 | 94.8 |
| ϕ | — | — | — | — | — | 78.7 | 78.5 | 91.8 |
| | — | — | — | — | — | — | 78.3 | 93.0 |
| t_c | — | — | — | — | — | — | — | 94.2 |

3.1. Evolution of Parameter Errors

The results in Table 1, Figure 1, and Table 2 demonstrate the improvement in parameter estimation when the merger and ringdown portions of the waveform are included. A related question is to ask how the parameter information accumulates with time. This is of great interest for the problem of searching for electromagnetic (EM) counterparts for MBHB mergers. If the final portion of the signal provides significant improvement in parameter estimates, there will be pressure to reduce the latency between LISA and EM observatories. This could affect decisions on data downlink operations, inter-spacecraft communications, and other aspects of the mission.

Figure 2 shows the effect of varying the upper cutoff frequency of the inner product in (6) on the SNR, D_L , θ , and ϕ . From the EM counterpart search perspective, these (along with perhaps t_c) are the most critical parameters. Since our waveforms are composed of a single mode, the GW frequency and $(t - t_c)$ can be related analytically [21]. Included on the plots in Figure 2 are points corresponding to $(t - t_c) = 1 \text{ min.}, 1 \text{ hr.}, 1 \text{ day}, \text{ and } 1 \text{ wk.}$ Figure 1 indicates that θ and ϕ improve by more than an order of magnitude in the final day before merger. Lang & Hughes [22] looked at spinning, precessing, unequal mass binaries using PN waveforms and found that sky position error decreased by similar amount during the final day before merger.

3.2. Effect of Mass

As a test of the effect of total redshifted system mass on our parameter estimation results, we simulated an ensemble of 140 equal mass, non-spinning MBHBs with $M = 10^7 M_\odot$ and $D_L = 6 \text{ Gpc.}$ Table 3 gives a summary of the mean and median parameter errors for this run. Comparing with the analogous ensemble of $M = 10^6 M_\odot$ systems summarized in Table 1, the heavier systems generally exhibit a reduced SNR and increased parameter errors. This can be explained by the shift of the GW signal to lower frequencies and its obscuration by the steeply-rising noise of the LISA detector. As with the $M = 10^6 M_\odot$ systems, the reduction in parameter errors with the inclusion of the merger signal is still present in the $M = 10^7 M_\odot$ case.

4. Conclusion

The results presented above indicate that inclusion of the merger signal can have a significant impact on LISA's ability to measure source parameters. It is interesting to compare this effect with other effects that have been studied previously. In Table 4, we compare our results for $M = 10^6 M_\odot$ at $z = 1$ with prior published works. The parameters compared are the fractional luminosity distance $D_L/D_L^{\text{true}} = \ln(D_L)$ and the solid angle subtended by the error ellipse, Ω_N . The latter quantity can be computed from the sky position angles, their errors, and their covariance. Aside from the differences in the waveform physics (spin, merger, etc.), the biggest difference in the studies is the length of the waveforms. Ours are a factor of ~ 30 shorter than those

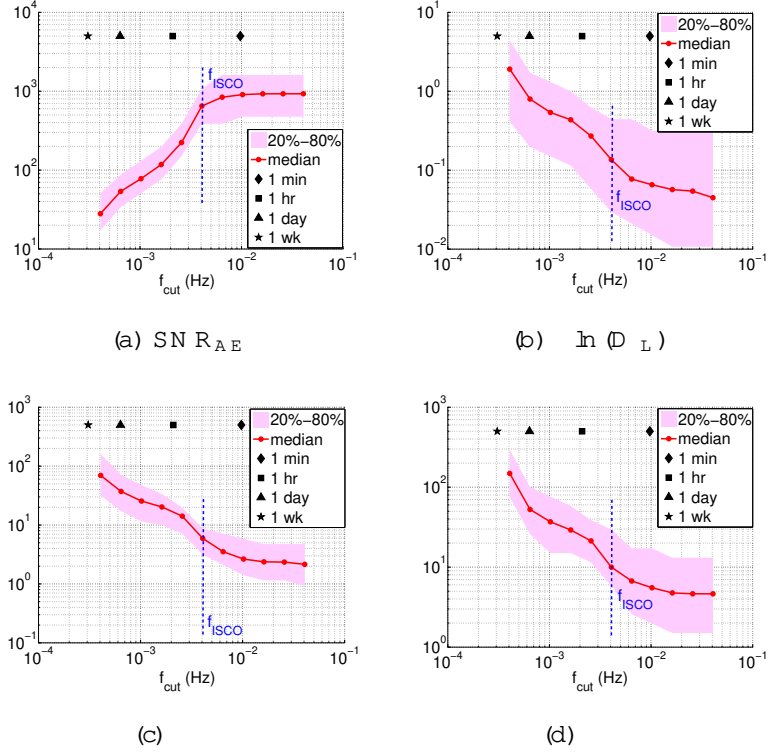


Figure 2. Effect of upper frequency cut on SNR, D_L , θ , and ϕ for the ensemble summarized in Table 1. Solid line denotes median values while shaded spans 20th to 80th percentile range. The vertical dashed line denotes the Schwarzschild ISCO frequency. Individual solid markers denote time before merger.

Table 3. Same as Table 1 for an ensemble of 140 equal-mass, non-spinning binaries with $M = 10^7 M_\odot$ at $D_L = 6 \text{ Gpc}$ ($z = 1$).

| | total mean | pre-ISCO mean | total median | pre-ISCO median |
|---------------------------|-------------------|-------------------|----------------------|-------------------|
| SNR_{AE} | 98.5 | 26.8 | 85.2 | 22.9 |
| $\ln(M = M_\odot)$ | $1.55 \cdot 10^6$ | $2.66 \cdot 10^6$ | $1.01 \cdot 10^6$ | $1.89 \cdot 10^6$ |
| $\ln(D_L = 1 \text{ pc})$ | 2.17 | 2.83 | $8.04 \cdot 10^{-1}$ | 1.07 |
| (deg) | 22.4 | 33.5 | 19.8 | 27.6 |
| (deg) | 58.4 | 103 | 22.0 | 35.1 |
| (deg) | 9.65 | 25.2 | $5.88 \cdot 10^{-1}$ | 1.40 |
| ι (deg) | $1.58 \cdot 10^3$ | $2.80 \cdot 10^3$ | 33.3 | 43.9 |
| (deg) | $1.62 \cdot 10^3$ | $2.87 \cdot 10^3$ | 79.9 | 111 |
| t_c (sec) | 14.7 | 77.2 | 13.1 | 68.5 |

Table 4. Comparison of source location for equal-mass MBHBs at $z = 1$ in this work to prior published works. S, P, and M refer to waveforms with spin, spin precession, and merger respectively. (δ estimated from the results in Table II of [4], δ^y estimated from histograms in FIG. 2 of [5])

| | M ($10^6 M_\odot$) | duration (yr) | S | P | M | δ_N (deg ²) | $D_L = D_L$ |
|-------------------|----------------------|---------------|-----|-----|-----|--------------------------------|----------------------|
| Cutler[4] | 4.0 | 1.0 | no | no | no | $4 \cdot 10^{-1}$ | $7 \cdot 10^{-2}$ |
| Vecchio[5] | 4.0 | 1.0 | no | no | no | $6 \cdot 10^{-1y}$ | $2 \cdot 10^{-2y}$ |
| Vecchio[5] | 4.0 | 1.0 | yes | no | no | $3 \cdot 10^{-1y}$ | $6 \cdot 10^{-3y}$ |
| Lang & Hughes[22] | 1.2 | 1.5 (avg) | yes | yes | no | $5.56 \cdot 10^{-2}$ | $3.57 \cdot 10^{-3}$ |
| this work | 1.0 | 0.03 | no | no | no | $5.08 \cdot 10^{-1}$ | $1.18 \cdot 10^{-1}$ |
| this work | 1.0 | 0.03 | no | no | yes | $1.13 \cdot 10^{-1}$ | $4.48 \cdot 10^{-2}$ |

used in the other published works due to the computational effort required to simulate long waveforms with Synthetic LISA.

The best comparison that can be made with this work is to compare the non-spinning results of Cutler and of Vecchio to our pre-ISCO case. $D_L = D_L$ is a factor of $2 - 5$ larger in our results than the published results. When the merger is added, the three results for $D_L = D_L$ approximately agree. This suggests that observing the final 10 days of a $M = 10^6 M_\odot$ MBHB at $z = 1$ will constrain D_L equally as well as observing the entire year prior to ISCO.

The results for δ_N for the short waveforms are considerably worse. This is consistent with the picture that modulations due to LISA's orbital motion provide much of the sensitivity to these parameters. Nevertheless, the improvement in δ_N upon inclusion of the merger is a factor of ~ 5 , roughly the same factor as the inclusion of spin precession.

Whether this same level of improvement will persist when long-duration observations, spin, and precession are added will depend on the exact mechanism by which the improvement arises. If both improvements result from breaking the same parameter degeneracy, then the improvement is likely to be minimal. If however, the mechanisms for improvement are orthogonal, it is possible that the relative improvement upon including the merger will be similar to the case here.

Acknowledgments

Copyright (c) 2008 United States Government as represented by the Administrator of the National Aeronautics and Space Administration. No copyright is claimed in the United States under Title 17, U.S. Code. All other rights reserved. This research was supported by an appointment to the NASA Postdoctoral Program at the Goddard Space Flight Center, administered by Oak Ridge Associated Universities through a contract with NASA.

References

- [1] Baker et al. Technical Report LISA-LIST-RP-436, 2007. v1.0.
- [2] M. Volonteri. AIP Conf. Series, 873:61{69, 2006.
- [3] D.E. Holz and S.A. Hughes. Ap.J., 629:15{22, 2005.
- [4] C. Cutler. Phys. Rev. D, 57:7089{7102, 1998.
- [5] A. Vecchio. Phys. Rev. D, 70(042001), 2004.
- [6] R.N. Lang and S.A. Hughes. Phys. Rev. D, 74(122001), 2006.
- [7] K.G. Arun, B.R. Iyer, B.S. Sathyaprakash, S. Sinha, and C. Van Den Broeck. Phys. Rev. D, 76(104016), 2007.
- [8] E.K. Porter and N.J. Cornish. Phys. Rev. D, 78(064005), 2008.
- [9] J.G. Baker, J. Centrella, D.I. Choi, M. Koppitz, and J. van Meter. Phys. Rev. D, 73(104002), 2006.
- [10] M. Campanelli, C.O. Lousto, and Y. Zlochower. Phys. Rev. D, 73(061501(R)), 2006.
- [11] J.G. Baker, S.T. McWilliam, J.R. van Meter, J. Centrella, D. Choi, B.J. Kelly, and M. Koppitz. Phys. Rev. D, 75(124024), 2007.
- [12] J.I. Thorpe. 211th Meeting of the Am. Astron. Soc., Jan 2008.
- [13] S. Babak, M. Hannam, S. Husa, and B. Schutz. (arXiv:0806.1591v1 [gr-qc]), June 2008.
- [14] S.L. Larson. Phys. Rev. D, 66(062001), 2002.
- [15] M. Tinto and J.W. Armstrong. Phys. Rev. D, 59(102003), 1999.
- [16] A. Krolak, M. Tinto, and M. Vallisneri. Phys. Rev. D, 70(022003), 2004.
- [17] T.A. Prince, M. Tinto, S.L. Larson, and J.W. Armstrong. Phys. Rev. D, 66(122002), 2002.
- [18] M. Vallisneri. Phys. Rev. D, 71(022001), 2005.
- [19] S.E. Timpano, L.J. Rubbo, and N.J. Cornish. Phys. Rev. D, 73(122001), 2006.
- [20] M. Vallisneri. Phys. Rev. D, 77(042001), 2008.
- [21] L. Blanchet. Living Rev. Relativity, 9(4), 2006.
- [22] R.N. Lang and S.A. Hughes. Ap.J., 677(2):1184{1200, 2008.